Published in final edited form as:
Anal Chem. 2007 June 15; 79(12): 4390–4400.

Structure and DNA Hybridization Properties of Mixed Nucleic Acid/Maleimide-ethylene glycol Monolayers

Chi-Ying Lee[1,3], **Phuong-Cac T. Nguyen**[1,2], **David W. Grainger**[4,5], **Lara J. Gamble**[1,2], and **David G. Castner**[1,2,3,*]

1 *National ESCA and Surface Analysis Center for Biomedical Problems, Box 351750 University of Washington, Seattle, WA 98195-1750*

2 *Departments of Bioengineering and Chemical Engineering, Box 351750 University of Washington, Seattle, WA 98195-1750*

3 *Departments of Pharmaceutics, University of Utah, Salt Lake City, UT 84112-5820*

4 *Departments of Pharmaceutical Chemistry, University of Utah, Salt Lake City, UT 84112-5820*

5 *Departments of Bioengineering, University of Utah, Salt Lake City, UT 84112-5820*

Abstract

The surface structure and DNA hybridization performance of thiolated single-strand DNA (HS-ssDNA) covalently attached to a maleimide-ethylene glycol disulfide (MEG) monolayer on gold have been investigated. Monolayer immobilization chemistry and surface coverage of reactive ssDNA probes were studied by X-ray photoelectron spectroscopy (XPS) and time-of-flight secondary ion mass spectrometry (ToF-SIMS). Orientation of the ssDNA probes was determined by near edge X-ray absorption fine structure (NEXAFS). Target DNA hybridization on the DNA-MEG probe surfaces was measured by surface plasmon resonance (SPR) to demonstrate the utility of these probe surfaces for detection of DNA targets from both purified target DNA samples and complex biological mixtures such as blood serum. Data from complementary techniques showed that immobilized ssDNA density is strongly dependent on the spotted bulk DNA concentration and buffer ionic strength. Variation of the immobilized ssDNA density had a profound influence on the DNA probe orientation at the surface and subsequent target hybridization efficiency. With increasing surface probe density, NEXAFS polarization dependence results (followed by monitoring the N 1s → π^* transition) indicate that the immobilized ssDNA molecules reorient towards a more upright position on the MEG monolayer. SPR assays of DNA targets from buffer and serum showed that DNA hybridization efficiency increased with decreasing surface probe density. However, target detection in serum was better on the “high density” probe surface than on the “high efficiency” probe surface. The amount of target detected for both ssDNA surfaces were several orders of magnitude poorer in serum than in purified DNA samples due to non-specific serum protein adsorption onto the sensing surface.

Keywords

ALKYLTHIOLATE MONOLAYERS; DNA; ESCA; GOLD SURFACES; HYBRIDIZATION; MALEIMIDE; MICROARRAY; NEXAFS; NUCLEIC ACID; ORIENTATION; PLASMON RESONANCE; SERUM; SURFACE CHARACTERIZATION; THIOLS; XANES; XPS

*Corresponding Author: David G. Castner, Director, National ESCA and Surface Analysis Center for Biomedical Problems, Departments of Bioengineering and Chemical Engineering, Box 351750, University of Washington, Seattle, WA 98195-1750. Email: castner@nb.engr.washington.edu, Telephone: 206-543-8094. Fax: 206-543-3778.

INTRODUCTION

Surface-bound single-stranded oligonucleotide (ssDNA) microarrays are powerful tools for large-scale parallel analysis of genome sequences and gene expression in biological and biomedical research.[1–3] Substantial effort is directed at fabrication and development of microarray and related biosensing surfaces. Nonetheless, no commercial microarrays offer levels of selectivity permitting the detection of nucleotide sequences without preliminary sample manipulation (i.e., purification, digestion, ligation or extension) and PCR amplification steps.[4] Thus, DNA microarray and biosensor technologies must be improved to reach full maturity and performance expectations. Specifically, device sensitivity and selectivity must be improved to permit direct target sequence detection from patient samples in real-time without the requirement for preliminary processing of target samples.

Currently, fluorescence imaging is most commonly used to analyze and detect target hybridization on DNA microarray surfaces.[5] Although traditional fluorescence-based DNA detection has a number of attractive features (e.g., broad availability and ease of use), the complex reagent labeling processes present several problems (e.g., poor reproducibility) and are time consuming,[6] and surface-derived fluorescence signal itself is subject to many measurement issues that preclude accurate quantitation of analyte. Label-free detection techniques such as surface plasmon resonance (SPR) spectroscopy and SPR imaging,[7–10] quartz crystal microbalance (QCM)[11, 12] and electrochemical DNA biosensors[13, 14] provide a more direct method of assay and avoid fluorescence metric issues. Nonetheless, use of these biosensing techniques for direct, label-free detection of DNA or RNA hybridization from complex biological samples requires that surface-capture DNA probes be optimally immobilized on a surface and resist nonspecific adsorption of other species from the biological fluid that contribute to assay noise.

On gold-coated SPR surfaces, DNA probe immobilization is most often accomplished through thiolate-gold bonds[15–20] formed by spontaneous reaction of thiolated ssDNA (HS-ssDNA) with the gold surface. Tarlov *et al.*[15] developed a widely used scheme to diminish non-specific interaction of the DNA probes with the gold surface by 'backfilling' the pure ssDNA adlayer with a short alkylthiol diluent mercaptohexanol (MCH) after thiolated DNA oligomer adsorption. Although hydroxyl-terminated alkylthiol treatment improved DNA target capture capability by preventing non-complementary DNA molecules from binding non-specifically to the probe surface from purified buffer solution, these ssDNA surfaces were not sufficiently protein resistant to perform assays in complex biological milieu.[21]

Recently, we have demonstrated that direct SPR capture of DNA targets from two complex media (blood serum and genomic DNA mixtures) is possible with the incorporation of a more protein resistant oligo(ethylene glycol) (OEG) thiol diluent.[22] Target hybridization from undiluted, unpurified serum and genomic DNA mixtures was detectable using OEG diluents in the probe-DNA surface, but one drawback of this system is the potential for the longer OEG diluent to sterically block target access to the lower base regions of the immobilized ssDNA probe, reducing full, stable target hybridization. This is consistent with the low DNA hybridization efficiencies (<50%) observed experimentally on these adlayers, even at low surface probe densities.[22]

To improve DNA hybridization from complex media, we have investigated the surface structure and performance of HS-ssDNA immobilized on maleimide-ethylene glycol disulfide (MEG) monolayers on gold. A number of studies have employed maleimide-thiol chemistry to attach HS-ssDNA to siliceous surfaces, due to its stability in aqueous environments and selectivity toward sulfhydrl groups. However, the conventional approach for the derivatization

of surfaces with maleimide groups involves multiple surface reactions: the preparation of an amino-terminated layer followed by reaction with a bifunctional linker molecule that contains both an amino-reactive site and a maleimide group.[23–30] Multiple steps, and potential side reactions between alkylsilanes, linker maleimides and amines could lead to undesired, uncontrolled chemistry on the surface;[2, 26] thus, this multi-step silane-based conjugation method does not offer acceptable control over surface maleimide density. Additionally, these maleimide surfaces do not offer sufficient resistance toward non-specific interactions with proteins or DNA molecules,[23] therefore are not well-suited for analysis of target molecules from complex biological milieu.

The MEG thiolate monolayers used in this study for DNA probe immobilization were formed via a single-step solution self-assembly of maleimide-ethylene glycol-terminated disulfides onto gold. The combination of minority surface-exposed maleimide functional moieties within a background of inert ethylene glycol groups has many advantages, including selective and efficient reactivity toward thiol ssDNA endgroups together with resistance to non-target DNA and proteins. X-ray photoelectron spectroscopy (XPS) and time-of-flight secondary ion mass spectrometry (ToF-SIMS) were used to characterize each surface modification step and resulting MEG monolayer structure on gold. A systematic XPS study was also performed to determine the dependence of DNA probe immobilization density on solution HS-ssDNA concentration and buffer ionic strength. DNA probe orientation was determined by near edge X-ray absorption fine structure (NEXAFS). Target DNA hybridization on these DNA-MEG probe surfaces was monitored by SPR to demonstrate their utility for detection of DNA targets from complex biological samples (e.g., blood serum) by determining the effects of non-specific adsorption on DNA hybridization. Quantification of target hybridization over a range of target concentrations (10 nM to 1 μM) in serum was studied to assess target detection limits in complex media.

EXPERIMENTAL SECTION

Materials

Silicon wafers (Silicon Valley Microelectronics, Inc., San Jose) and low-fluorescence SF-14 glass slides (Schott Glass Technology, Durea, PA) were used as substrates. Maleimide-ethylene glycol-terminated disulfide [HO-$(CH_2$-CH_2-$O)_4$-$(CH_2)_{11}$-S-S-$(CH_2)_{11}$-$(O$-CH_2-$CH_2)_6$-OCH_2-CONH-$(CH_2)_2$-$C_4H_2NO_2$] (MEG) was purchased from Prochimia (Sopot, Poland). Mercapto-1-hexanol [HS-$(CH_2)_6$-OH] was purchased from Sigma-Aldrich. High performance liquid chromatography (HPLC)-purified DNA oligomers [HS-ssDNA: 5′-HS-$(CH_2)_6$-CTGAACGGTAGCATCTTGAC-3′, complementary target: 5′-GTCAAGATGCTACCGTTCAG-3′, and non-complementary target: 5′-CTGAACGGTAGCATCTTGAC-3′] were purchased from TriLink Biotechnologies (San Diego, CA). Thiolated DNA oligomers from this vendor were previously shown to contain minimal contaminants that interfere with HS-ssDNA surface assembly.[31] Tris(2-carboxyethyl)phosphine (TCEP, neutral pH) disulfide bond cleavage solution was purchased from Pierce (Rockford, IL). DNA probe immobilization buffer, denoted as SSC, contained 1.5M NaCl (Fisher, Fair Lawn, NJ) and 0.015M sodium citrate (J.T. Baker, Phillipsburg, NJ), pH 7.0. DNA hybridization buffer, denoted as STE, contained 1.0M NaCl (Fisher, Fair Lawn, NJ), 10mM Tris-HCl (Sigma, St. Louis, MO), and 1mM ethylenediaminetetraacetic acid (EDTA, Fisher) and was adjusted to pH 7.4 by adding 1.0M NaOH. Fetal bovine serum (FBS, Premium, US Origin, Hybridoma Screened, 14–901F, Lot 01103197, total protein 35–60 mg/ml) was purchased from Cambrex (Baltimore, MD), stored at −80°C until use and diluted with STE to 50% concentration (by volume) prior to hybridization experiments.

DNA immobilization on maleimide-ethylene glycol SAMs

Silicon wafers used for XPS, ToF-SIMS and NEXAFS experiments were coated with 10 nm titanium and 100 nm gold (99.99%) by electron beam evaporation at pressures below 1×10^{-6} Torr. Glass slides used for SPR experiments were coated with 2 nm chromium and 50 nm gold (99.99%) under identical conditions. (Specific chemistry used for the attachment of HS-ssDNA is shown in Figure 1.) In step 1, MEG monolayers were prepared by immersing freshly gold-coated substrates in ethanolic solutions containing 0.1mM MEG disulfides for 1 hour at room temperature. After formation of the MEG adlayer, samples were removed from the solution, rinsed with ethanol and blown dry with N_2. In step 2, HS-ssDNA solutions were prepared in 0.2 to 2M SSC buffer (pH 7) at concentrations ranging from 5 to 500μM to study the effects of ionic strength and probe solution concentration on immobilized DNA density. DNA probe solutions (20μl for XPS, ToF-SIMS and NEXAFS samples and 80μl for SPR samples) were treated with TCEP (0.2mM) for 30 minutes, spotted with a micropipette on the MEG SAMs formed from the first step (spot sizes approximately 5 and 10mm in diameter) and incubated at room temperature under 100% humidity for 1.5 h (XPS analysis indicated little difference between immobilization of DNA from 1.5 h to 24 h; data not shown. Note that the spotted DNA solution did not evaporate even after 24 h of incubation). Spotted DNA samples were then rinsed repeatedly with SSC buffer and Millipore water to remove non-specifically bound DNA oligonucleotide probes and then immersed in a solution of 0.5mM MCH in 2M SSC buffer (pH 7) for 30 min to block unreacted maleimide groups. To verify that HS-ssDNA was covalently linked to the surface via thiol reactions with the maleimide C=C bond, negative controls consisting of (1) MEG SAMs exposed to non-thiolated DNA (30 and 100μM) in 2M SSC for 24 hrs and (2) MEG SAMs pre-treateded with 0.5mM MCH followed by exposure to HS-ssDNA (30 and 100μM) in 2M SSC for 24 hrs have been analyzed in parallel. All samples were blown dry with N_2 and stored under N_2 until analysis.

X-ray photoelectron spectroscopy (XPS)

XPS data were acquired using a Kratos AXIS Ultra DLD spectrometer with a monochromated Al-Kα X-ray source. All compositional measurements were acquired at a photoelectron take-off angle of 0° in “hybrid mode” (take-off angle is defined as the angle between the sample surface normal and the axis of the XPS analyzer lens). The typical X-ray spot size was 700 μm × 300 μm. For each sample, an initial compositional survey scan was acquired, followed by detailed (P2p, N1s, O1s and S2p) scans using a pass energy of 80eV. Angle-resolved compositional data were acquired at photoelectron take-off angles of 0°, 55° and 75° in “electrostatic mode”. The acceptance angle in this mode is about 12 degrees which corresponds to sampling depths of approximately 10, 5 and 2nm for of 0°, 55° and 75° take-off angles, respectively. Detailed (P2p, N1s, O1s, S2p, C1s, and Au4f) scans were acquired using a pass energy of 80eV at each take-off angle. High-resolution C1s spectra were also acquired using a pass energy of 20eV at 0° and 75° take-off angles. The number of scans taken at different angles was adjusted to optimize the signal-to-noise ratio. Two or more replicates of each sample were analyzed and averaged to obtain the reported atomic percent (at%) values. Data analysis was performed with Vision Processing data reduction software (Kratos Analytical Ltd.) and CasaXPS (Casa Software Ltd.).

Time-of-flight secondary ion mass spectrometry (ToF-SIMS)

ToF-SIMS data were acquired on a Physical Electronics PHI 7200 time-of-flight spectrometer using an 8keV Cs^+ primary ion source in the pulsed mode. Spectra were acquired for both positive and negative secondary ions over a mass range of (m/z) 0–1000. The area of analysis for each spectrum was 100μm × 100μm, and the total ion dose was maintained below 2×10^{12} ions/cm^2. Mass resolutions ($m/\Delta m$) were typically 6000 and 5000 for the (m/z) 27 and 25 peaks in the positive and negative spectra, respectively. Three spots on two replicates of each

sample were analyzed. Positive ion spectra were mass calibrated using the CH_3^+, $C_2H_3^+$ and $AuSCH_2^+$ peaks, and negative ion spectra were mass calibrated using the CH^-, C_2H^- and AuS^- peaks. Mass calibration errors were kept below 10 ppm. Principal component analysis (PCA) was performed on ToF-SIMS data as described previously[32] using a series of scripts written by NESAC/BIO for MATLAB (MathWorks, Inc., Natick, MA). Prior to PCA, a peak list was created including all peaks that were at least 3 times the background for the given region as well as some peaks related to the fragmentation of the DNA molecules which have previously been reported.[31, 33] All spectra were normalized to the sum of the intensities of the selected peaks and mean-centered to ensure that the variance in the data set was due to differences in sample variances rather than differences in sample means.

Near edge X-ray absorption fine structure (NEXAFS)

NEXAFS spectra were taken at the National Synchrotron Light Source (NSLS) U7A beamline at Brookhaven National Laboratory. This beam line uses an ~85% polarized, high intensity beam, a monochromator and 600 l/mm grating which gives a full-width at half-maximum (FWHM) resolution of ~0.15eV at the carbon K-edge (~285eV).[34] The monochromator energy scale was calibrated using the C1s → π^* transition of graphite, located at 285.35eV.[35] The effects of incident beam intensity fluctuations and monochromator absorption features were eliminated by normalizing all NEXAFS spectra to the signal from a pure gold (gold deposited *in situ*) mesh (I_0). Partial electron yield (PEY) was monitored by a channeltron electron multiplier with an adjustable entrance grid bias (EGB). The bias voltage was maintained at −150V for carbon K-edge spectra and −360V for nitrogen K-edge spectra. Samples were mounted to allow rotation about the vertical axis to change the angle between the sample surface and the incident X-ray beam. The NEXAFS angle is defined as the angle between the incident X-ray beam and the sample surface. A near normal incident beam is defined as the X-ray striking the surface at an angle of 70° from the sample surface while a glancing incident beam is generally 20° from the surface plane. The electric field vector (E) is perpendicular to the X-ray incident beam. A disordered system on the sample surface does not show any polarization dependence because of the random orientation of the molecules. Polarization dependence is indicative of directional alignment of the molecules in the overlayer.[35, 36]

Surface plasmon resonance (SPR)

Details of the SPR measurements have been described previously.[22] Briefly, this SPR system is based on a planar prism (Kretschmann) configuration. The glass side of the gold-coated substrate is index-matched to the prism while the functionalized surface is mechanically pressed against a milled Teflon™ flow cell. A polychromatic light beam is passed through the prism and the backside of a gold-coated substrate to excite surface plasmon waves at the metal-dielectric interface. The reflected light is analyzed with a spectrograph. [Note that the spotted DNA probe region (~10mm in diameter) is larger than the analysis area.] During SPR measurements, STE buffer and target DNA solutions (1 μM complementary and non-complementary control DNA strands in STE buffer) were sequentially delivered to the SPR surface of immobilized DNA probes at a flow rate of 50 μl/min. Interactions at the gold surface were observed by monitoring the wavelength shift of the SPR reflected minimum. SPR optical data was converted to quantitative units (adsorbed mass per unit area) using the method published by Jung *et al.*[37]

RESULTS AND DISCUSSION

XPS analysis of the DNA-immobilized surfaces

MEG SAM and immobilized ssDNA film composition—XPS analysis was used to verify the surface composition of the maleimide-ethylene glycol self-assembled monolayers (MEG SAMs) and the subsequently immobilized ssDNA. The XPS-determined elemental

compositions for each stage of the DNA probe immobilization chemistry are summarized in Table 1. Survey scans of MEG SAMs indicated the presence of all elements expected from the MEG disulfide (i.e., N, O, C, and S) and substrate (Au), with no additional elements. Surface composition of the MEG SAMs given as atomic percentages (at%) (77at% C, 18at% O, 3at% N, and 1at% S, renormalized without the gold substrate signal) were close to their expected theoretical compositions (75at% C, 19at% O, 3at% N, and 3at% S) predicted by molecular stoichiometry with the exception of sulfur. Sulfur atomic percent is lower than theoretically expected due to its position within the adlayer at the gold surface, its signal attenuated by the MEG overlayer. After ssDNA immobilization onto the MEG SAM, the most notable compositional change is the appearance of the P2p signal (1.2 at%) attributed to DNA attachment at the surface. No phosphorus signal was detected from MEG SAMs exposed to identical immobilization buffer, incubation, and post-immobilization steps, without HS-ssDNA present (Table 1). Consistent with detection of the P2p signal, nitrogen signal also increased from the presence of nitrogen-containing DNA bases. Decrease in gold at% suggests masking of substrate signal as DNA overlayers form during immobilization.

An important consideration is the possibility of ssDNA attaching to the surface through the Michael addition with amine groups in DNA bases. Such side reactions could lead to unfavorable probe orientation on the surface for target hybridization.[38, 39] To investigate the specificity of the DNA immobilization reaction, MEG SAMs were treated for 24 h with solutions containing non-thiolated ssDNA (100μM in 2M SSC). XPS results (Table 1) show no significant difference in the elemental compositions of the MEG SAMs before and after exposure to non-thiolated DNA. Hence, DNA chains lacking terminal thiols do not attach to the MEG SAMs even after 24 hours of incubation in high salt concentration, confirming thiol ssDNA specificity with the immobilized maleimide groups. XPS results also showed that treatment of the MEG monolayer with mercapto-1-hexanol (0.5mM in 2M SSC) prevented subsequent immobilization of HS-ssDNA to the MEG SAMs (i.e., no P detected by XPS). XPS composition results demonstrate attachment of HS-ssDNA probes to the MEG SAMs through thiol reactions with the maleimide C=C bond. This end-tethered DNA orientation is expected to preserve the activity of bound DNA probe strands toward solutions containing complementary targets.[15, 16, 21, 22, 39]

MEG adlayer and immobilized ssDNA film structure determined by angle-resolved XPS—Angle-resolved XPS studies provided structural information for both MEG monolayers and the immobilized ssDNA overlayer. Data for three different take-off angles (0, 55, and 75°, sampling depths of approximately 10, 5 and 2nm, respectively) are shown in Figure 2 (further details in Table S1, Supporting Information). To effectively bind HS-ssDNA and resist non-specific adsorption during target hybridization, both maleimide and ethylene glycol chemistry should be exposed at the outer monolayer surface (see Figure 1). The presumed asymmetric distribution of nitrogen (from maleimide), oxygen (from ethylene glycol), and sulfur (from thiol) in the MEG adlayer provided a basis for monitoring monolayer surface structure on gold using changes in the nitrogen, oxygen, and sulfur intensities at the different XPS take-off angles. Both nitrogen and oxygen concentrations increased with increasing take-off angle (decreasing sampling depth), confirming that the maleimide and ethylene glycol portions of the MEG molecules are located at the outer surface of the MEG monolayer (for more details see Table S1, Supporting Information). This provides accessibility for HS-ssDNA reaction as well as resistance to non-target molecules. Consistent with the nitrogen and oxygen trends, the carbon and sulfur concentrations decreased with increasing take-off angle. High-resolution XPS C1s spectra measured at normal and glancing take-off angles are compared in Figures 2a and b. Carbon species from the MEG monolayer include C-C and C-H at 285eV, C-N and C-O at 286.5-287eV, and N-C(=O)-C at 289eV binding energies (BE), respectively. (Relative concentrations of the different C1s carbon species measured at each take-off angle are summarized in Table S2, Supporting Information.) The XPS-determined composition of

the carbon species at 0° (~10nm sampling depth, > full adlayer thickness) was close to the expected theoretical compositions. While intensities of the C-N/C-O and N-C(=O)-C peaks associated with maleimide increased at the higher glancing angles (most surface sensitive, < ~5nm depth), the hydrocarbon species intensity decreased. The high-resolution S2p spectrum measured at 0° take-off angle exhibited the expected doublet structure (e.g., from $S(2p_{3/2})$ and $S(2p_{1/2})$ peaks, Figure 2c), with the $S(2p_{3/2})$ BE at approximately 162eV, consistent with sulfur-gold thiolate species.[40] The $S(2p_{1/2})$ peak was 1.2eV higher in BE and with half the intensity of the $S(2p_{3/2})$ peak, as expected. No detectable sulfur intensity was present in the BE region above 164eV, confirming lack of sulfur oxidation and that MEG chains were bound to gold via thiol-gold interactions.

DNA probe immobilization to the maleimide produced modest increases in the relative nitrogen and oxygen concentrations and slight decreases in the carbon and sulfur concentrations at glancing take-off angle (details in Table S1, Supporting Information). The relative phosphorus concentration also increased towards glancing take-off angle, indicating DNA probe surface immobilization at the film surface. DNA addition resulted in minimal change in the C1s chemical species (details provided in Table S2, Supporting Information), attributed to the similar functional groups in both DNA-conjugated and un-conjugated MEG layers.

DNA probe immobilization efficiency and ionic strength dependence

Surface probe density has been shown to be an important DNA surface property that affects target hybridization efficiency.[15, 17, 21] Hence, it is important to identify and characterize factors affecting DNA surface density to control and optimize target capture. XPS compositional data were collected for HS-ssDNA immobilized at 0, 5, 10, 20, 30, 40, 50, 100, 250, and 500μM spotting probe concentrations and fixed ionic strength (1.5M SSC). Figure 3a shows relative amounts of surface-immobilized ssDNA oligomers tracked using XPS-determined phosphorus and nitrogen at%. DNA surface concentrations are proportional to XPS-determined N and P at% as shown in previously reported quantification methods for immobilized DNA on gold[21, 39, 41] as well as on other organically modified array substrates.[26, 42] However, due to the confounding presence of nitrogen in the MEG adlayer, only phosphorus is uniquely characteristic of DNA. No phosphorus was detected from the MEG layers for DNA spotting probe concentrations less than 30μM (Figure 3a). Above 30μM, DNA phosphorus at% for DNA-immobilized surfaces increases with increasing spotting probe solution concentration. Consistent with the increasing phosphorus at%, nitrogen at% also increased (Figure 3a) while the gold substrate signal decreased (data not shown) as DNA overlayers increase in density. DNA probe density on the MEG surfaces saturates at approximately 500μM spotting probe concentration. DNA probe surface density on the MEG adlayers is estimated by correlating XPS P2p at% to that previously reported for the DNA/mercaptoundecanol (MCU) samples calibrated by radiometric density measurements.[21] Estimated DNA probe densities on the MEG SAMs range from 2×10^{12} to 3×10^{13} molecules/cm^2 for the 30 to 500μM spotted bulk HS-ssDNA concentration range. These density values are in reasonable agreement with densities reported in earlier studies of thiol-terminated DNA immobilized onto maleimide supports.[24–30]

The types of salt and ionic strength of the buffer spotting solution have been reported to affect thiolated DNA assembly onto gold as well as for covalently immobilized ssDNA on polymer slides.[41, 42] Thus, experiments were performed with the spotted bulk HS-ssDNA concentration kept at 100μM while buffer salt concentration was varied from 0.2 to 2.0M. The XPS P2p and N1s at% from these MEG surfaces showed a strong dependence of DNA probe immobilization efficiency on buffer ionic strength (Figure 3b). At low ionic strengths (0.2 to 0.5M SSC), no phosphorous signal was detected from the MEG SAMs, indicating little or no DNA probe was immobilized. By increasing immobilization buffer concentration from 1.0 to

1.5M, relative amounts of immobilized DNA probe more than doubled, as indicated by the two-fold increase in P2p signal, while increasing from 1.0 to 2.0M increased immobilized DNA probe density almost 3-fold (Figure 3b) to 3×10^{13} molecules/cm^2. These results demonstrate an alternative method for adjusting the surface probe density on the MEG surfaces when limited amounts of DNA probe are available.

ToF-SIMS Analysis

Successful immobilization of HS-ssDNA onto MEG surfaces is also strongly supported by ToF-SIMS data. Peaks characteristic of the maleimide ($C_5H_4NO_2^+$ at m/z 110, $C_6H_6NO_2^+$ at m/z 124, $C_4H_2NO_2^-$ at m/z 96, etc.; for more details see Tables S3 and S4, Supporting Information for the selected peak m/z lists for all species) are present in the low mass range (m/z < 125) in both positive and negative ion spectra. Consistent with previous studies of ethylene glycol (EG) films,[43, 44] the expected characteristic EG peaks are also present in both positive and negative spectra ($C_2H_3O^+$ and $C_2H_3O^-$ at m/z 43, $C_2H_5O^+$ at m/z 45, $C_3H_7O^+$ at m/z 59, $C_2H_2O_2^-$ at m/z 58, etc.) of the MEG adlayers. Evidence for chemical bonding between maleimide and HS-ssDNA is obtained from peaks corresponding to the intact maleimide ring (m/z = 96.01, Figure 4a) and the maleimide ring to which a sulfur had been added (m/z = 127.98, Figure 4b) in the negative ion spectra. After DNA immobilization, the normalized intensity for the reacted maleimide species ($C_4H_2NO_2S^-$, m/z = 127.98) increased and normalized intensity for the unreacted maleimide species ($C_4H_2NO_2^-$, m/z = 96.01) decreased. The normalized peak intensity of the maleimide ring signal is a measure of the reactive maleimide groups available for reaction while the intensity of the sulfur-added maleimide ring is a measure of maleimide groups already reacted. Therefore, ToF-SIMS analysis supports some unreacted maleimide groups remaining in the MEG film after ssDNA immobilization. Notably, after MCH 'quenching' treatment, the reacted maleimide species normalized intensity increased while that from the unreacted maleimide decreased.

PCA was used to compare the negative ion ToF-SIMS data from the MEG films and those immobilized with ssDNA at various probe and buffer salt concentrations. Figure 4c shows a scores plot of principal component 1 (PC 1), capturing 89% of the data variance, versus P2p at% (from XPS), representative of ssDNA surface density. Results in Figure 4c indicate that the variation in the ToF-SIMS data was due primarily to differences in surface density of immobilized ssDNA. Comparison of the PC 1 loadings plot (Figure 4d) to the PC 1 scores indicates that the MEG samples are correlated with peaks originating from the maleimide (e.g., $C_4H_2NO_2^-$) and EG (e.g., C_2HO^- and $C_2H_3O^-$) while the immobilized ssDNA samples are correlated as might be predicted with the phosphate- and nitrogen-containing fragments such as adenine ($C_5H_5N_5$), guanine ($C_5H_5N_5O$) and thymine ($C_5H_6N_2O_2$) from the DNA.[31, 33] PCA results indicate that MEG films spotted with 30μM DNA resulted in lower DNA surface coverage compared to those spotted with 100μM DNA. Furthermore, more ssDNA was immobilized at higher ionic strength buffer (i.e., 2M SSC) compared to lower ionic strength buffer (i.e., 1.5M SSC). Hence, the results of PCA analysis agree well with XPS results for HS-ssDNA probe immobilization described in the previous section.

NEXAFS Analysis

NEXAFS analysis was employed to determine immobilized DNA orientation on the MEG surfaces with respect to the substrate surface. Figure 5a shows the N K-edge NEXAFS spectra for both MEG and ssDNA films obtained at 20° (glancing) and 70° (near normal) incidence angles. For the MEG surface (Figure 5a, spectra i), a sharp peak observed at ~402 eV is attributed to the N1s→ $\pi^*_{N\text{-}C=O}$ transition for the nitrogen found in the maleimide ring.[45, 46] Intensity of this feature between the 20° and 70° spectra does not change, indicating no preferential orientation of the maleimide groups at the surface.

After HS-ssDNA immobilization, a π^* doublet feature (ΔE = 1.7eV) is observed within the 399–402eV region of the NEXAFS N K-edge spectra (Figure 5a, spectra ii–iv). The π^* doublet feature represents an average signal over the four different nucleotide bases, as seen in spectra from a pure ssDNA monolayer on gold (Figure 5a, spectra v) and those previously reported for gold-bound ssDNA[39, 47, 48] and dsDNA.[49] The new π^* peak near 400eV is consistent with an "aromatic" nitrogen π^* peak for nitrogen atoms in a conjugated ring structure.[50, 51] The higher energy π^* peak at 401–402eV is due to the nitrogen atoms in the nucleobases located next to carbonyl groups.[47, 49] The broader peak above 405eV is attributed to the N 1s → σ* transition.[39, 47, 49]

The low-density ssDNA spectra (Figure 5a, spectra ii) showed a slight polarization dependence within the 399–402eV region. Transitions to π^* orbitals are slightly enhanced when the X-ray beam is at glancing angle of incidence to the sample surface (θ= 20°) where the electric field vector (E) of the polarized X-ray source is more perpendicular to the surface. Overlap of this E vector with the antibonding π^* orbitals of the DNA bases indicates that the bases are on average nominally parallel to the gold surface. With increasing DNA probe density at the surface, this polarization dependence increased. Changes in the orientation of the ssDNA with increasing surface probe density could be monitored by comparing the dichroic ratio, ΔN_{π}^*,[52, 53]:

$$\Delta N_{\pi^*} = \frac{N_{\pi^*,20^\circ} - N_{\pi^*,70^\circ}}{N_{\pi^*,20^\circ} + N_{\pi^*,70^\circ}}$$

Note that dichroic ratios calculated here are relative and cannot be directly compared across values from different experimental setups. Comparison of dichroic ratios derived from different experiments requires a correction factor 1/(2P-1), where P is the polarization degree of the synchrotron light.[52, 53] The ΔN_{π}^* values for the MEG films and immobilized ssDNA films of varying surface density are shown in Figure 5b. ΔN_{π}^* increased significantly with increasing DNA surface density. This is similar to previous results reported for mixed DNA/MCU and DNA/OEG monolayers where limited electrostatic repulsive interactions between ssDNA chains at lower ssDNA surface density permit more disorder among the DNA chains.[22, 39] In addition, ssDNA immobilized on the MEG SAMs showed higher ΔN_{π}^* (i.e., improved orientation and order) compared to that obtained from a pure ssDNA monolayer on gold. This indicates that the underlying ethylene glycol layer is able to prevent non-specific interactions between the nucleobase amine groups and the surface (as discussed in XPS section and shown previously by XPS and NEXAFS results[22]), thereby yielding an end-tethered DNA orientation at the surface. However, the ΔN_{π}^* ratios of all ssDNA-MEG samples were lower than the highest ΔN_{π}^* ratios observed previously for both DNA/MCU[39] and DNA/OEG[22] mixed monolayers on gold.

DNA Target Hybridization Density and Efficiency Measured by SPR assay

Hybridization measurements were obtained with SPR to provide quantitative information regarding target binding efficiency of DNA-modified MEG surfaces. In a first set of hybridization experiments, probe surfaces of varying ssDNA density ($2\pm0.3 \times 10^{12}$ to $3\pm0.4 \times 10^{13}$ molecules/cm^2, obtained by varying spotted bulk HS-ssDNA concentration and ionic conditions as described above) were exposed to non-complementary and complementary DNA strands in STE buffer. Four representative hybridization curves from these probe surfaces are shown in Figure 6a. Exposing DNA probe surfaces to non-complementary DNA solution showed no significant changes in SPR signals after buffer rinsing (Figure 6a, curve i). This indicates that the MEG surface effectively blocks non-complementary DNA non-specific surface adsorption. In contrast, exposing probe surfaces to complementary DNA targets produced complementary strand hybridization, evidenced by increases in SPR sensorgram signals above baseline (Figure 6a, curves ii–v). Target density on the probe surfaces ranged

from 1.6×10^{12} molecules/cm^2 for lowest density probe surfaces (~2×10^{12} molecules/cm^2, spotted with 30μM HS-ssDNA in 1.5M SSC) to 5.0×10^{12} molecules/cm^2 for highest density probe surfaces (spotted with 100μM HS-ssDNA in 2M SSC). Target hybridization efficiencies were derived as a percentage of probe molecules hybridized [(target density (by SPR)/probe density (by XPS)) × 100%] and presented in Figure 6b. Target hybridization efficiency varied with surface probe density as expected.[17, 21, 22, 26] A hybridization efficiency of ~90% was obtained for low probe density surfaces, agreeing with earlier reports[17, 26, 42] of hybridization efficiencies close to 100% on surfaces with DNA probe densities below 4×10^{12} molecules/cm^2. At 50μM probe spotting concentration and probe density of ~6×10^{12} molecules/cm^2, a lower hybridization efficiency was obtained (~45%). Further increase in probe density significantly reduced target hybridization efficiency to 15%. This reduced hybridization efficiency at higher probe coverage can be explained by charge-charge and steric effects: at high probe density, closely packed DNA probes produce high local electrostatic repulsion and steric hindrance to target DNA, preventing formation of stable duplexes on the surface.

As a test of this hypothesis, the ionic strength of the rinsing buffer was gradually reduced (from 1 to 0 M) after target hybridization. Amounts of hybridized target remaining on the surface were monitored by SPR in situ. Figure 6c shows percentages of hybridized targets remaining on the surface as a function of buffer salt concentration. By reducing ionic strength, increasing electrostatic repulsion between the hybridized strands resulted in reduced target densities on all probe surfaces. However, the amount of hybridized target on surface decreased more drastically for surfaces with high probe density (spotted with 100μM HS-ssDNA in 2M SSC) compared to those with low probe densities (spotted with 30μM HS-ssDNA in 1.5M SSC). Thus, it is clear that lower electrostatic repulsive interactions between DNA chains at lower DNA surface density facilitate stable duplexes upon removal of ions while higher probe density results in higher electrostatic repulsions that inhibit stable DNA duplexes to form in low ionic strength environments. These results are consistent with previous reports[17, 26, 42] and provide additional evidence that probe surface density plays an important role in target capture efficiency.

Although most hybridization experiments have been restricted to detection of purified target DNA sequences at high concentrations (i.e., 1μM), the ability to directly detect small amounts of specific nucleotide sequences in complex, contaminant-ridden samples without the use of exogenous reagents or procedures is desirable for direct sample-to-answer clinical/diagnostic applications. To address the challenge of real-life sample conditions where most solute burden does not correspond to the target DNA, SPR was used to investigate the amount of specific target capture on the DNA-MEG surface in blood serum spiked with 1μM, 100nM, and 10nM complementary DNA target. For comparison, the same experiments were performed in spiked buffer. Both “high efficiency” probe surfaces (i.e., surface spotted with 30μM HS-ssDNA in 1.5M SSC with a ~90% hybridization efficiency in buffer target DNA solutions) and “high density” probe surfaces (i.e., surface spotted with 100μM HS-ssDNA in 1.5 MSSC with ~20% hybridization efficiency in buffer target DNA solutions) were examined. As experimental controls for target hybridization in serum, the SPR response from serum samples containing non-complementary DNA sequences were also measured and subtracted as background from the SPR response from complementary DNA in serum (details for SPR measurement of target hybridization in serum is provided in Supporting Information). As seen in Figures 7a and b SPR data from buffer, concentrations of target DNA as low as 10nM were easily detected on both “high efficiency” and “high density” probe surfaces. The amount of target detected on both probe surfaces decreased only slightly as target concentration was reduced from 1μM to 10nM. Exposing probe surfaces to complementary DNA targets in serum resulted in significant decreases in amounts of target detected. For “high efficiency” probe surface, target captured at 1μM target concentration was reduced by ~70% compared to that detected from buffer, due to non-specific serum protein adsorption (Figure 7a). As target concentration in serum was

further reduced to 100nM, no significant target hybridization was detected on the "high efficiency" probe surface. By contrast, on "high density" probe surfaces complement target hybridization at 1μM target concentration was only reduced by ~30% compared to hybridization in buffer (Figure 7b). SPR measurements showed that 7×10^{11} target DNA/cm^2 was detected at 100nM target concentration in serum on the high density, low efficiency probe surface. However, no significant target hybridization was detected at 10nM target concentration in serum due to rapid, overwhelming amounts of non-specific protein adsorption onto the probe surface. Comparison of Figure 7a with Figure 7b shows that 100nM target DNA in serum was detectable on the "high density" probe surface and not the "high efficiency" surface. The observed differences in target hybridization on the two probe surfaces are likely due to different amounts of probe molecules available for target binding. "High density" probe surfaces contain more than double the number of available probes compared to "high efficiency" surface. Thus, at high levels of non-specific protein adsorption on each surface, probes on the "high efficiency" surface will be blocked before probes on the "high density" surface. Different target capture performance observed for the "high efficiency" and "high density" surfaces does not appear to be due to differences in their resistance to non-sepefic protein adsorption since both surfaces adsorbed similar amounts of protein (~2 nm SPR signal shift). Although target detection in serum is improved on the "high density" probe surface over the "high efficiency" probe surface, the amount of target captured on both surfaces from 10nM target concentrations are several orders of magnitude poorer in complex biological mixtures compared to purified DNA samples.

CONCLUSIONS

Complementary surface analytical techniques show that immobilized ssDNA density is strongly dependent on spotted bulk DNA concentration and buffer ionic strength. Different immobilization densities ranging from 2×10^{12} to 3×10^{13} molecules/cm^2 resulting from varying these two immobilization conditions profoundly influence DNA probe surface orientation and subsequent target hybridization efficiency. With increasing surface probe density, NEXAFS polarization dependence results show reorientation of immobilized ssDNA molecules towards a more upright position on the MEG monolayer. SPR measurements demonstrated the utility of these surfaces to capture DNA targets from complex biological samples such as blood serum and the substantial detrimental effects of non-specific adsorption on DNA hybridization signal. Quantitative target hybridization measured over a range of target concentrations (10nM to 1μM) in buffer and serum showed target detection in serum is better on "high density" probe surfaces (i.e., those spotted with 100μM HS-ssDNA in 1.5M SSC with a target hybridization efficiency of ~20% in pure target DNA buffer solutions) than on "high efficiency" probe surfaces (i.e., those spotted with 30μM HS-ssDNA in 1.5M SSC with a target hybridization efficiency of ~90% in pure target DNA buffer solutions). However, the amount of target captured for both assay formats are several orders of magnitude poorer in complex biological mixtures than in DNA buffer samples due to non-specific serum protein adsorption onto the sensing surface. These differences demonstrate the current challenge for direct sample-to-answer nucleic acid capture assays in the presence of substantial competing non-specific adsorption. Assays will rely on improved detection formats and control of DNA probe surface chemistry to provide selective and sensitive performance in point-of-care diagnostics, thereby addressing clinical and field assay requirements not met by current PCR-based assay platforms.

Supplementary Material

Refer to Web version on PubMed Central for supplementary material.

Acknowledgements

The authors gratefully acknowledge support from NESAC/BIO (NIH Grant No. EB-002027) and NIH Grant EB-001473. We also thank J.S. Apte and D.A. Fischer for their technical assistances with the NEXAFS experiments. NEXAFS studies were performed at the NSLS, Brookhaven National Laboratory, which is supported by the U.S. Department of Energy, Division of Materials Science and Division of Chemical Sciences.

References

1. Lamartine J. Mater Sci Eng C-Biomimetic Supramol Syst 2006;26:354–359.
2. Wang YY, Prokein T, Hinz M, Seliger H, Goedel WA. Anal Biochem 2005;344:216–223. [PubMed: 16061196]
3. Debouck C, Goodfellow PN. Nature Genet 1999;21:48–50. [PubMed: 9915501]
4. Hahn S, Mergenthaler S, Zimmermann B, Holzgreve W. Bioelectrochemistry 2005;67:151–154. [PubMed: 16019267]
5. Livache T, Maillart E, Lassalle N, Mailley P, Corso B, Guedon P, Roget A, Levy Y. J Pharm Biomed Anal 2003;32:687–696. [PubMed: 12899959]
6. Churchill GA. Nature Genet 2002;32:490–495. [PubMed: 12454643]
7. Wolf LK, Fullenkamp DE, Georgiadis RM. J Am Chem Soc 2005;127:17453–17459. [PubMed: 16332097]
8. Piliarik M, Vaisocherova H, Homola. J Biosens Bioelectron 2005;20:2104–2110.
9. Shumaker-Parry JS, Aebersold R, Campbell CT. Anayl Chem 2004;76:2071–2082.
10. Wark AW, Lee HJ, Corn RM. Anayl Chem 2005;77:3904–3907.
11. Lazerges M, Perrot H, Zeghib N, Antoine E, Compere C. Sens Actuator B-Chem 2006;120:329–337.
12. Su XD, Wu YJ, Knoll W. Biosens Bioelectron 2005;21:719–726. [PubMed: 16242610]
13. He PA, Xu Y, Fang YZ. Anal Lett 2005;38:2597–2623.
14. Rivas GA, Pedano ML, Ferreyra NF. Anal Lett 2005;38:2653–2703.
15. Herne TM, Tarlov MJ. J Am Chem Soc 1997;119:8916–8920.
16. Levicky R, Herne TM, Tarlov MJ, Satija SK. J Am Chem Soc 1998;120:9787–9792.
17. Peterson AW, Heaton RJ, Georgiadis RM. Nucleic Acids Res 2001;29:5163–5168. [PubMed: 11812850]
18. Aqua T, Naaman R, Daube SS. Langmuir 2003;19:10573.
19. Letsinger RL, Mirkin CA, Elghanian R, Mucic RC, Storhoff JJ. Phosphorus Sulfur Silicon Relat Elem 1999;146:359–362.
20. Demers LM, Ginger DS, Park SJ, Li Z, Chung SW, Mirkin CA. Science 2002;296:1836–1838. [PubMed: 12052950]
21. Gong P, Lee CY, Gamble LJ, Castner DG, Grainger DW. Anayl Chem 2006;78:3326–3334.
22. Lee CY, Gamble LJ, Grainger DW, Castner DG. Biointerphases 2006;1:82–92.
23. Wu P, Hogrebe P, Grainger DW. Biosens Bioelectron 2006;21:1252–1263. [PubMed: 16002276]
24. Wang YY, Cai J, Rauscher H, Belun RH, Goedel WA. Chem-Eur J 2005;11:3968–3978.
25. Vaidya AA, Norton ML. Langmuir 2004;20:11100–11107. [PubMed: 15568863]
26. Shen G, Anand MFG, Levicky R. Nucleic Acids Res 2004;32:5973–5980. [PubMed: 15537837]
27. Shen G, Horgan A, Levicky R. Colloid Surf B-Biointerfaces 2004;35:59–65.
28. Strother T, Cai W, Zhao XS, Hamers RJ, Smith LM. J Am Chem Soc 2000;122:1205–1209.
29. Brockman JM, Frutos AG, Corn RM. J Am Chem Soc 1999;121:8044–8051.
30. Chrisey LA, Lee GU, Oferrall CE. Nucleic Acids Res 1996;24:3031–3039. [PubMed: 8760890]
31. Lee CY, Canavan HE, Gamble LJ, Castner DG. Langmuir 2005;21:5134–5141. [PubMed: 15896061]
32. Wagner MS, Castner DG. Langmuir 2001;17:4649–4660.
33. May CJ, Canavan HE, Castner DG. Anayl Chem 2004;76:1114–1122.
34. Lenhart JL, Jones RL, Lin EK, Soles CL, Wu WL, Fischer DA, Sambasivan S, Goldfarb DL, Angelopoulos MJ. Vac Sci Technol B 2002;20:2920–2926.

35. Morar JF, Himpsel FJ, Hollinger G, Jordon JL, Hughes G, McFeely FR. Phys Rev B 1986;33:1346–1349.
36. Stohr, J. NEXAFS Spectroscopy. Springer-Verlag; New York: 1992.
37. Jung LS, Campbell CT, Chinowsky TM, Mar MN, Yee SS. Langmuir 1998;14:5636–5648.
38. Huang E, Zhou F, Deng L. Langmuir 2000;16:3272–3280.
39. Lee CY, Gong P, Harbers GM, Grainger DW, Castner DG, Gamble LJ. Anayl Chem 2006;78:3316–3325.
40. Castner DG, Hinds K, Grainger DW. Langmuir 1996;12:5083–5086.
41. Petrovykh DY, Kimura-Suda H, Whitman LJ, Tarlov MJ. J Am Chem Soc 2003;125:5219–5226. [PubMed: 12708875]
42. Gong P, Harbers GM, Grainger DW. Anayl Chem 2006;78:2342–2351.
43. Wagner MS, Pasche S, Castner DG, Textor M. Anayl Chem 2004;76:1483–1492.
44. Lu HB, Campbell CT, Castner DG. Langmuir 2000;16:1711–1718.
45. Urquhart SG, Hitchcock AP, Priester RD, Rightor EG. J Polym Sci Pt B-Polym Phys 1995;33:1603–1620.
46. Urquhart SG, Hitchcock AP, Leapman RD, Priester RD, Rightor EG. J Polym Sci Pt B-Polym Phys 1995;33:1593–1602.
47. Samuel NT, Lee CYL, Gamble LJ, Fisher DA, Castner DG. Journal of Electron Spectroscopy and Related Phenomenon 2006;152:134–142.
48. Petrovykh DY, Perez-Dieste V, Opdahl A, Kimura-Suda H, Sullivan JM, Tarlov MJ, Himpsel FJ, Whitman LJ. Journal of the American Chemical Society 2006;128:2–3. [PubMed: 16390092]
49. Crain JN, Kirakosian A, Lin JL, Gu YD, Shah RR, Abbott NL, Himpsel FJ. Journal of Applied Physics 2001;90:3291–3295.
50. Shard AG, Whittle JD, Beck AJ, Brookes PN, Bullett NA, Talib RA, Mistry A, Barton D, McArthur SL. Journal of Physical Chemistry B 2004;108:12472–12480.
51. Zwahlen M, Brovelli D, Caseri W, Hahner G. Journal of Colloid and Interface Science 2002;256:262–267.
52. Zharnikov M, Ouchi Y, Hasegawa M, Scholl A. J Phys Chem B 2004;108:859–863.
53. Samant MG, Stohr J, Brown HR, Russell TP, Sands JM, Kumar SK. Macromolecules 1996;29:8334–8342.

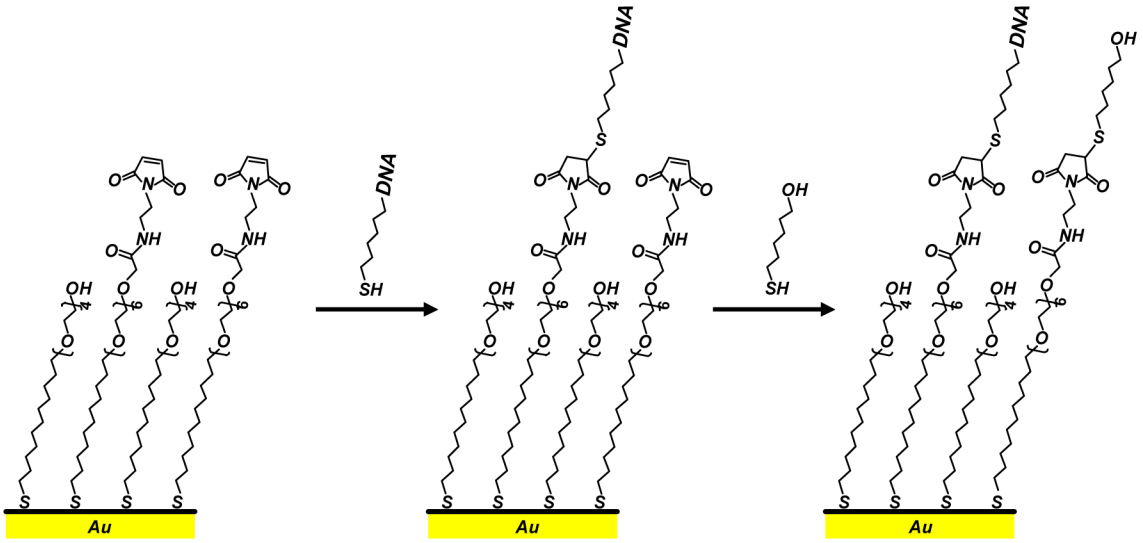

Figure 1.
Scheme for immobilization of thiolated, single-stranded DNA (HS-ssDNA) onto a maleimide-ethylene glycol disulfide (MEG) monolayer on gold. The maleimide reacts selectively with the thiol endgroup on the DNA while the ethylene glycol moieties prevent non-specific adsorption of non-target molecules to the probe surface.

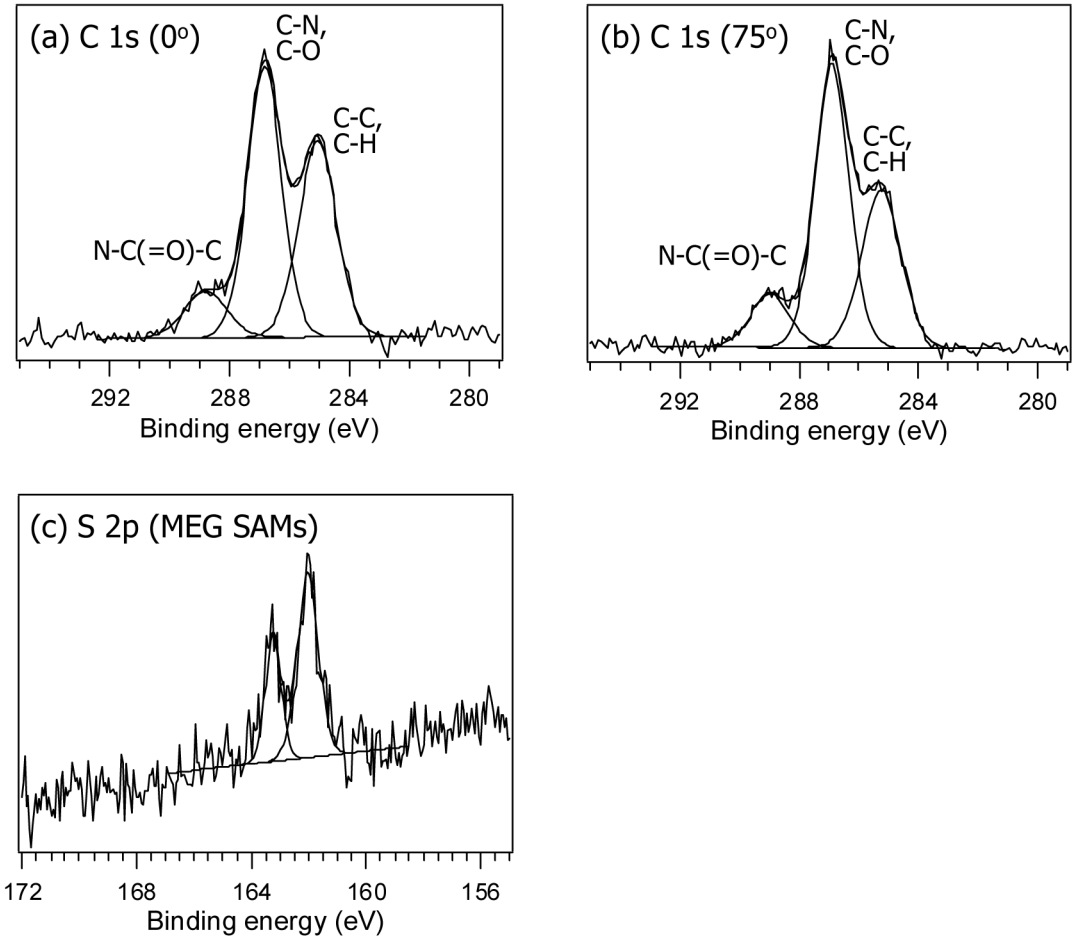

Figure 2.

MEG monolayer on gold XPS analysis. Angle-resolved, high-resolution (a) C1s spectrum at 0° take-off angle (~10nm), (b) C1s spectrum at 75° take-off angle and (c) S2p spectrum at 0° take-off angle and peak fits used for area measurements. Peak binding energies for high-resolution spectra were referenced to the Au 4f peak at 84.0eV. Intensities of the C-N/C-O and N-C(=O)-C peaks increased at glancing angle while hydrocarbon species peak intensity decreased. High-resolution S2p spectra measured at 0° take-off angle exhibited a doublet structure from overlapping S($2p_{3/2}$) and S($2p_{1/2}$) peaks. The binding energy (BE) of the S ($2p_{3/2}$) peak (162 eV) is consistent with sulfur-gold surface thiolate species.[40]

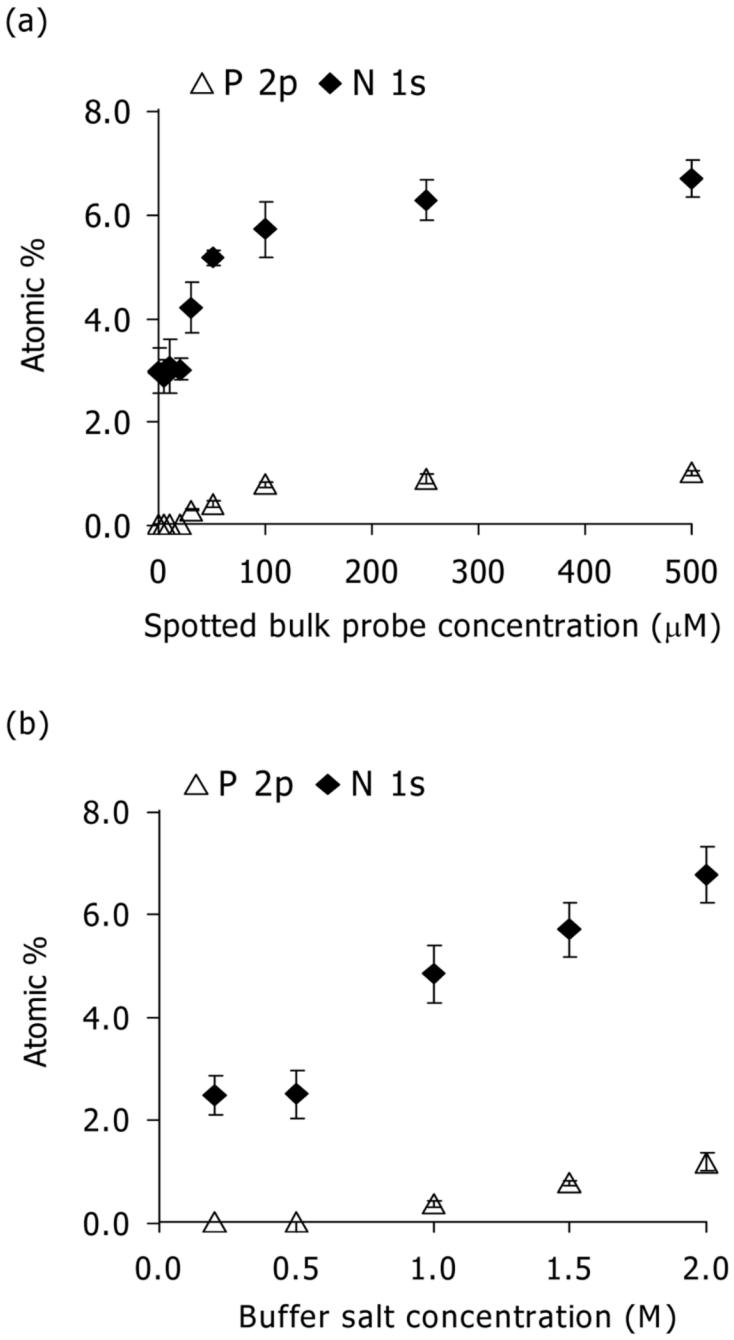

Figure 3.

DNA probe immobilization dependence on (a) bulk DNA probe concentration (in 1.5M SSC buffer) and (b) buffer ionic strength (with 100μM DNA) studied using XPS. Relative amounts of immobilized ssDNA have been expressed as P2p (open triangles) and N1s (closed diamonds) atomic percents (at%). No P2p signal was detected from MEG surfaces for spotting probe concentrations less than 30μM. Beyond 30μM, the P2p and N1s at% for DNA-immobilized MEG films increases with increasing spotting probe solution concentration. A strong dependence of immobilization efficiency on buffer salt content was observed. By increasing immobilization buffer concentration from 1.0 to 1.5M, the P2p and N1s at% from immobilized

DNA probe more than doubled, while increasing buffer strength from 1.0 to 2.0M increased immobilized DNA probe density almost 3-fold.

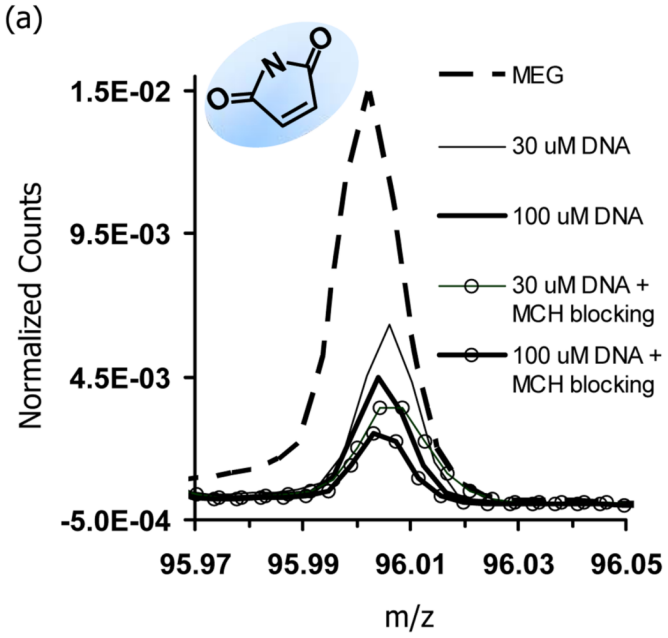

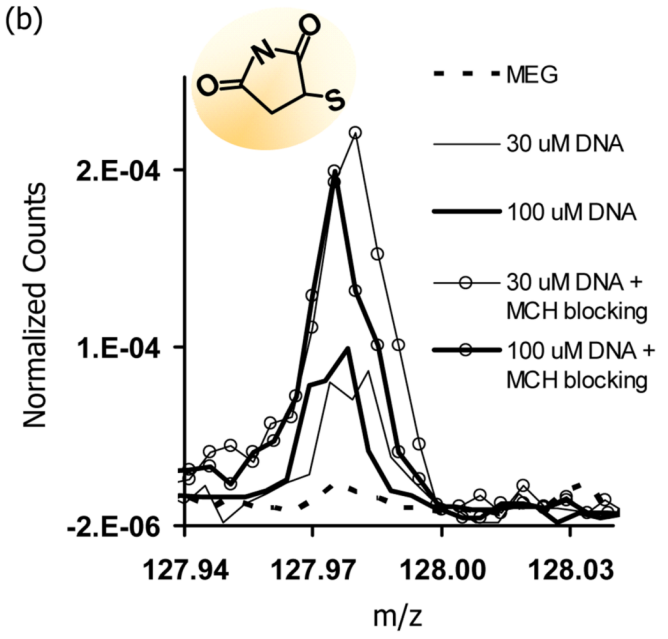

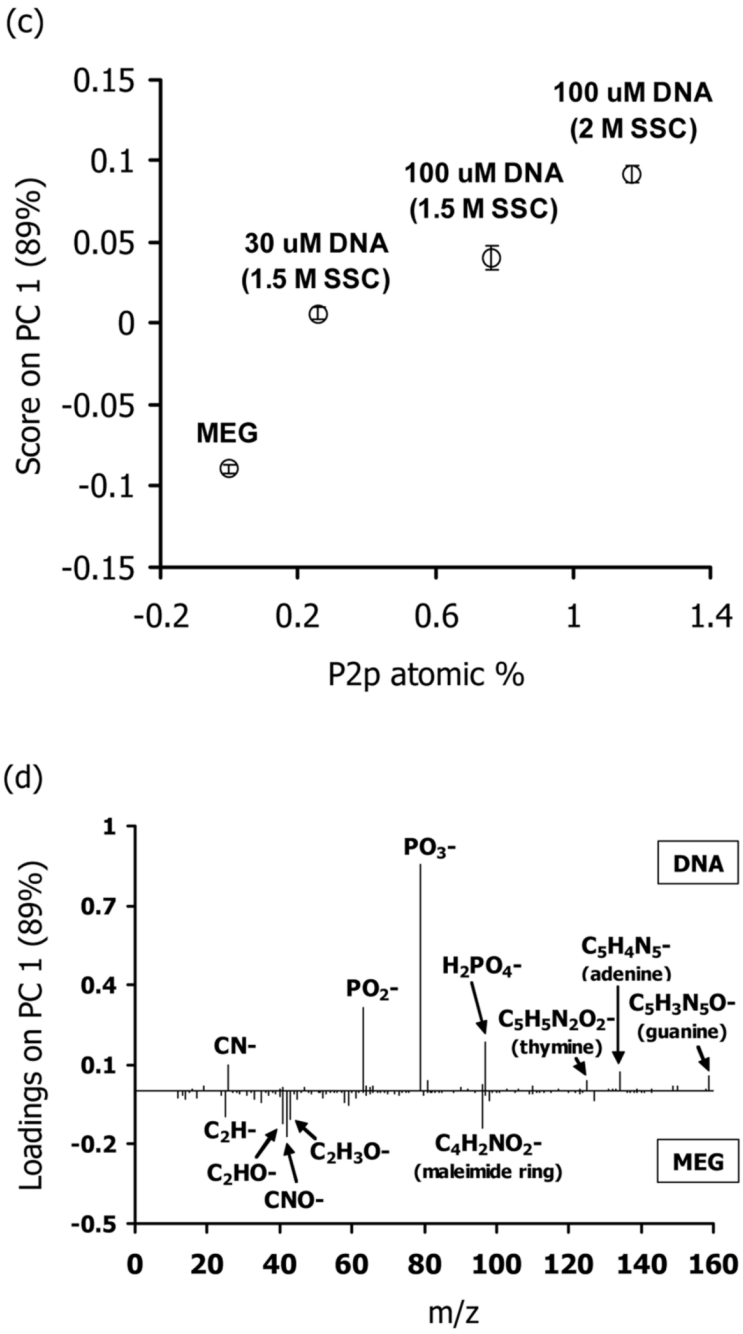

Figure 4.

Evolution of the normalized negative ion ToF-SIMS peaks corresponding to unreacted maleimide (m/z = 96.01) (a) and thiol-reacted maleimide (m/z = 127.98) (b) for the MEG monolayer on gold, immobilized DNA (30 and 100μM HS-ssDNA in 1.5 and 2M SSC, respectively) and immobilized DNA treated with MCH. Peaks were normalized to the total ion intensities. PC1 scores (c) and loadings (d) plots for the negative ion ToF-SIMS data. (c) PC1 scores: The vertical axis shows the PC score, and the horizontal axis shows the P2p atomic% obtained from XPS. PC1 for the negative data captures 89% of the variance in the data and, as seen, can separate the spectra from MEG films and DNA films prepared using different HS-ssDNA spotting concentrations and buffer ionic strengths. (d) PC1 loadings: The vertical axis

shows the PC loadings, and the horizontal axis shows peak mass. For clarity, only a few peaks are labeled on the plot. Peaks that load positively in the PC 1 loadings plot (d) correspond with samples with positive scores on PC 1 in the scores plot (c) and vice versa. PC 1 effectively separates the MEG SAM from the DNA samples as a result of phosphate and nitrogen-containing molecular fragments originating from the DNA.

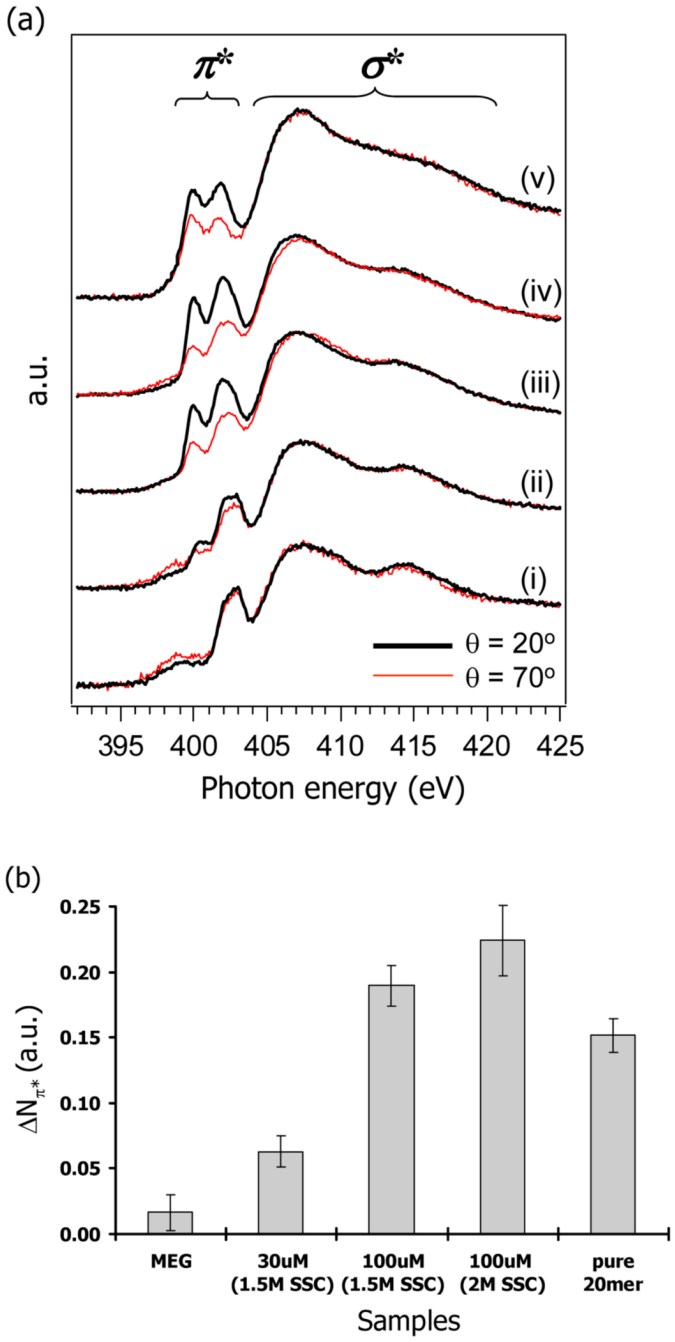

Figure 5.

Nitrogen K-edge NEXAFS spectra (a) from MEG monolayers (i), MEG monolayers spotted with 30μM DNA in 1.5M SSC (ii), 100μM DNA in 1.5M SSC (iii) and 100μM DNA in 2M SSC (iv) and pure ssDNA monolayers on gold (v) at near normal (70°) and glancing (20°) incident X-ray angles. Lack of polarization dependence for the N K-edge spectra of the MEG monolayer (i) indicates no preferential orientation of the terminal maleimide groups. After DNA immobilization, a $_{\pi}$* doublet feature (ΔE = 1.7eV), which represents an average signal over the four different nucleotide bases as seen in the spectra from a pure ssDNA monolayer on gold (v) is observed within the 399–402eV region of spectra ii–iv. The low-density ssDNA spectra (ii) showed slight polarization dependence, indicating that DNA bases are on average

nominally parallel to the gold surface. With increasing DNA probe density at the surface (iii and iv), this polarization dependence increased. Dichroic ratio (ΔN_{π}^{*}) for MEG monolayer and immobilized DNA on MEG SAMs versus directly onto gold (b). DNA immobilized on the MEG monolayers showed higher ΔN_{π}^{*} (i.e., improved orientation and order) in comparison to that obtained from a pure ssDNA monolayer on gold.

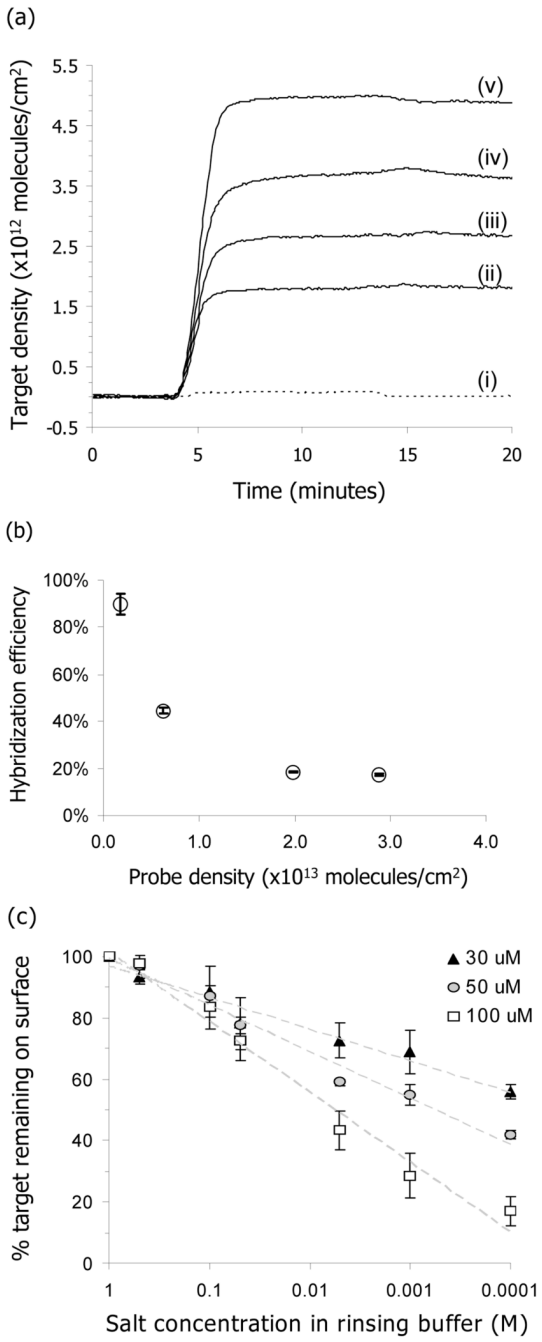

Figure 6.

Real-time SPR assays of target capture specificity from buffer (a). A measurement baseline was established by introducing buffer to the probe surfaces at 0 min. At 5 min, non-complementary (i) and complementary (ii–v) DNA sequences were flowed over MEG monolayers spotted with (i and ii) 30μM DNA in 1.5M SSC, (iii) 50μM DNA in 1.5M SSC, (iv) 100μM DNA in 1.5M SSC and (v) 100μM DNA in 2M SSC, but only the complementary DNA strand hybridized. As DNA hybridization approached saturation, the DNA solution was replaced with buffer to rinse away loosely bound DNA molecules from the probe surface. Data indicate that target surface density increases with increasing probe density. Estimated hybridization efficiency for each DNA/MEG probe surface as a function of surface probe

density (b). Percentage of hybridized targets remaining on the surface as a function of buffer ionic strength (c). Reduced ionic strength increased electrostatic repulsion between hybridized strands, resulting in reduced target densities on all probe surfaces.

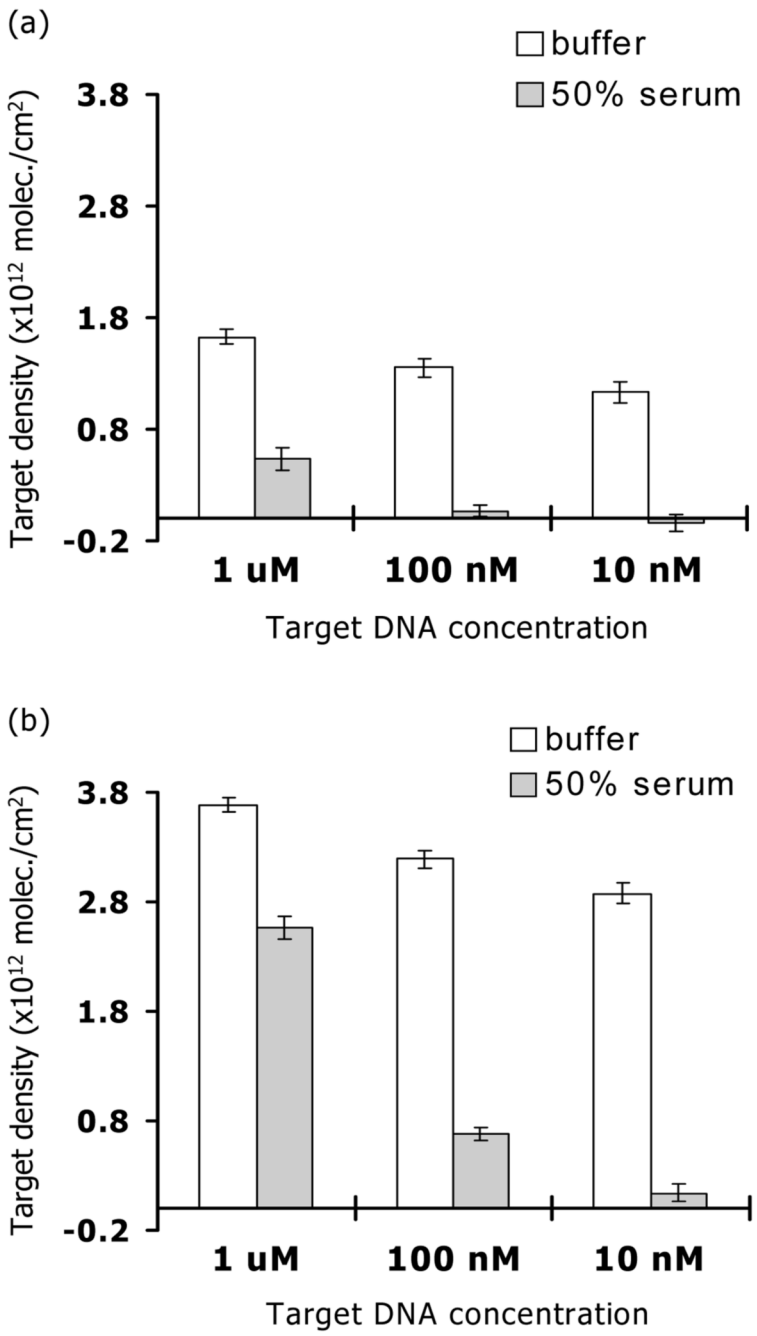

Figure 7.

Target hybridization on DNA-MEG probe surfaces measured by SPR in buffer and blood serum spiked with 1μM, 100nM, and 10nM complementary DNA target for a “high efficiency” surface (a) and “high density” surface (b). SPR data indicate that target capture in serum are better on the “high density” probe surfaces than on the “high efficiency” probe surfaces but for a 10nM target concentration are several orders of magnitude poorer than in buffer for both probe surfaces.

Table 1

XPS-determined elemental compositions for each stage of the DNA probe immobilization chemistry and from control samples

Sample	Atomic Percent (Std. dev)					
	Au 4f	**C 1s**	**O 1s**	**N 1s**	**S 2p**	**P 2p**
MEG monolayer on gold	17.4 (1.4)	63.8 (1.6)	15.1 (0.7)	2.8 (0.4)	0.9 (0.1)	0.0 (0.0)
+ immobilization buffer	17.6 (0.6)	64.8 (0.9)	13.8 (0.5)	3.0 (0.6)	0.8 (0.1)	0.0 (0.0)
+ thiolated DNA (100μM in 1.5M SSC, 1.5 h incubation)	12.5 (0.4)	63.5 (1.2)	16.4 (0.6)	5.7 (0.5)	1.2 (0.2)	0.8 (0.1)
+ thiolated DNA (100μM in 1.5M SSC, 1.5 h incubation) + MCH blocking	12.8 (0.4)	65.1 (0.4)	14.9 (0.4)	5.1 (0.4)	1.1 (0.2)	0.9 (0.1)
+ non-thiolated DNA (100μM in 2M SSC, 24 h incubation)	17.4 (0.2)	64.7 (0.5)	14.1 (0.1)	3.0 (0.6)	0.8 (0.2)	0.0 (0.0)
+ MCH + thiolated DNA (100μM in 2M SSC, 24 h incubation)	19.7 (1.0)	62.3 (0.6)	14.0 (0.6)	2.5 (0.1)	1.4 (0.0)	0.0 (0.0)